Transition pathways between solid and liquid state in suspensions

Lutz Heymann and Nuri Aksel*

Department of Applied Mechanics and Fluid Dynamics, University of Bayreuth, D-95440 Bayreuth, Germany

(Received 26 July 2006; revised manuscript received 18 December 2006; published 27 February 2007)

Suspensions containing rigid monodisperse spherical particles in a Newtonian carrier liquid are investigated experimentally, providing evidence for solid and liquid states in a transient shear rate from rest. Between these two states a transition takes place; the transition pathways from solid to liquid and from liquid to solid being different. The dynamics of the transition are shown, with the material in this regime reacting as a highly nonlinear system. This involves inverting the input to output and vice versa and comparing them. A key feature of the transition regime is a material instability caused by the collapse of the particle network structure.

DOI: 10.1103/PhysRevE.75.021505 PACS number(s): 82.70.−y, 83.80.Hj, 64.70.Dv, 83.50.−v

I. INTRODUCTION

Highly concentrated suspensions are materials with a complex rheological behavior which is, in general, a combination of elastic, viscous, and plastic components, that has its origin in the properties of both the dispersed phase and the carrier liquid as well as in their interaction [1].

One of the most controversially important and historical material parameters associated with the study of suspensions is the yield stress [2–6], commonly regarded as one fixed single scalar parameter. In the physical sense the yield stress is assumed to act as a switch between the no-flow and the flow region, i.e., between solidlike and liquidlike behavior. Recently, Varnik *et al.* [7] have studied the yield stress of a binary Lennard-Jones glass theoretically by means of molecular dynamic simulations and found an overshoot of the shear stress in the stress-strain relation for various constant total shear rates. Below this maximum they obtained a solidlike behavior with a linear range at very low strains commensurate with the experiments of Zhu *et al.* [8].

Although the yield stress is not uniquely defined in the literature (see, e.g., [8,11] and references therein), the solidlike behavior below the yield stress is usually modeled as a linear elastic (Hookean) solid [9,10], while the liquidlike behavior above the yield stress is often modeled with linear (Bingham) or nonlinear constitutive equations (e.g., Herschel-Bulkley, Casson), sometimes combined with time-dependent effects.

From an experimental perspective the yield stress and the related solid-liquid transition cause some difficulties; under certain circumstances the yield stress leads to sheared and unsheared regions, with a sharp solid-liquid interface in geometries with an inhomogeneous shear field, e.g., in coaxial cylinder geometries [12,13]. Similar effects due to shear banding, with no sharp border between unsheared and sheared regions or due to inhomogeneous strain fields, have been observed by magnetic-resonance-imaging (MRI) rheometric experiments [14] and by optical visualization techniques [15] in truncated cone-and-plate geometries with large cone angles.

Currently, in contrast to the solid and liquid regimes, the material behavior in the transition region is not well-understood. There are only a few papers in the literature dealing with the transition regime in which a phase change takes place which is always coupled with structural change [16]. The latter, which results in a more-or-less pronounced nonmonotonous, or discontinuous behavior in the constitutive relationship, is denoted as an intrinsic material instability [17,18]. Picard *et al.* [19] associated the nonmonotonous flow curves with local inhomogeneities in a macroscopically homogenous shear field. Møller *et al.* [11] combined the concept of yield stress with thixotropy and under certain conditions found nonunique flow curves with a local shear stress minimum; in this case the yield stress is no longer a fixed material property but depends on the mechanical history of the material.

As stated by Goddard [18], experimental data concerning flow curves for real suspensions with an intrinsic material instability due to phase transition are still missing in the literature; the aim of the present investigation is to understand the complex transition pathways between the solid and the liquid state. For this, it is necessary to prove the existence of solid and liquid states. The existence of a local maximum in the stress-strain or stress-strain rate curves is verified experimentally. Since it is still unclear if the transition from solid to liquid state is the same as the reverse transition this too is explored. Furthermore, the open question as to the influence of the experimental mode on the reaction of the material is considered; the similarities and, especially, the differences in the material behavior of suspensions under transient controlled shear rate (TCSR) and transient controlled shear stress (TCSS) are investigated.

II. MATERIAL AND METHODS

A. Materials and sample preparation

To understand the solid-liquid transition clearly, free from the influence of complicating factors, simply composed suspensions with well-known properties were used, comprised of nonporous spherical polymethylmetacrylate (PMMA) particles (having a density of $\rho_D = 1190\ \mathrm{kg/m^3}$ at 20 °C) dispersed in a low molecular weight polydimethylsiloxane (PDMS) solution (with a density $\rho_S = 970\ \mathrm{kg/m^3}$ and a dynamic viscosity $\eta_S = 216$ mPa s at 20 °C). Use of the latter guaranteed the experiments to be free from evaporation ef-

*Corresponding author. Electronic address: tms@uni-bayreuth.de

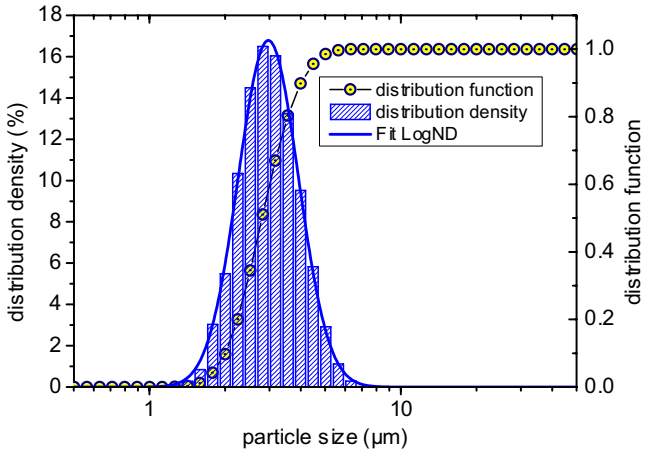

FIG. 1. (Color online) Particle size distribution of PMMA particles.

fects. Also, since the densities of the two phases differ only by 18.5% and due to the high solid volume concentrations involved, the resulting suspensions were found to be stable against demixing and sedimentation for periods greater than 1 month; so much so, that even in the small gaps of the instruments used to measure their properties, settling effects could justifiably be considered negligible.

The particle size distribution (PSD) was measured by laser light diffraction with a Mastersizer 2000 (Malvern Instruments Ltd., Worcestershire, UK) based on Mie scattering, with the complex refractive index of PMMA given by $r_i = 1.524 + 0.01i$, and is shown in Fig. 1 as a logarithmic normal distribution (log ND) with a mean diameter $d_{\text{mean}} = 3.2\ \mu\text{m}$ and a standard deviation $s = 0.138\mu\text{m}$. Hence the polydispersity [20]

$$\xi = \frac{1.645s}{d_{\text{mean}}} \tag{1}$$

has a value of 0.071 and the PSD is quasimonodisperse.

The Newtonian behavior of PDMS was confirmed by measuring the dynamic viscosity at 20 °C over a shear rate range 10^{-1} to $10^{3}\ \text{s}^{-1}$ using a rotational rheometer MCR500 (Anton Paar, Germany) having a concentric double gap cylinder system.

Before preparing the suspensions, the particles were dried in a vacuum at a temperature of 60 °C for 4 h in order to remove any residual water. A master batch suspension, with a solid volume concentration of 60%, was manufactured by manual mixing of both components before being homogenized in a three-roller mill for 5 min. Suspensions with various solid volume concentrations were then produced as required from the master batch by dilution with the appropriate quantity of carrier liquid.

B. Rheological devices, methods, and preshear

Experiments were performed using both a controlled strain or strain rate (CSR), Advanced Rheometric Expansion System (ARES) rheometer (Rheometric Scientific Inc., now TA Instruments Ltd.) equipped with a Force Rebalance Transducer 2KFRTN1 and a Modular Compact Rheometer MCR500 (Anton Paar Germany), utilizing in both cases a truncated cone-and-plate geometry having a diameter of 50 mm and a cone angle of 0.01745 rad, and with a minimum gap setting of approximately 50 μm. Accordingly, the ratio of the latter to the mean particle size was greater than 15 which is sufficiently large for the assumption that the continuum hypothesis holds to be satisfied.

Comparison of results obtained with both rough and smooth measuring geometries showed no significant differences, indicating wall slip as a possible source of errors can be ignored. This was further verified by performing oscillatory measurements at various strain amplitudes. The associated amplitude spectra calculated from the shear stress response signal [21] did not feature any even harmonics, proving conclusively that wall slip had no influence on the flow curves presented in subsequent sections (see, e.g., [21,22]).

Inertia effects were minimized by proper calibration [23,24] and the induction of high normal stresses during filling and closing eliminated as described by Heymann *et al.* [21]. Because mechanical history influences the rheological behavior of a sample, an equal starting state for each is necessary prior to measurement, which is achieved by a proper preshear [21].

III. RESULTS AND DISCUSSION

A. Transient controlled shear rate (TCSR) mode

As a precursor to proof of a local maximum of the shear stress it is important to consider the solidlike and liquidlike rheological behavior of different suspensions in terms of their uniquely defined corresponding flow, $\sigma = f_l(\dot{\gamma})$, and deformation, $\sigma = f_s(\gamma)$, curves for different ramp times t_R, as plotted in Fig. 2. The ramp time t_R is given by

$$\dot{\gamma}(t) = \dot{\gamma}_0 \left(\frac{\dot{\gamma}_\infty}{\dot{\gamma}_0} \right)^{t/t_R}, \tag{2}$$

with $\dot{\gamma}_0$ and $\dot{\gamma}_\infty$ as initial and final shear rates of the TCSR experiment.

Note that, for each solid volume concentration, the flow and deformation curves show the data for one and the same experiment. The flow curve for the pure carrier liquid is shown as a solid line for comparison purposes. Such plots provide unambiguous evidence of the existence of both solid and liquid phases and give new insights into the material behavior at very low and high shear rates or strains, respectively, as shown by Heymann *et al.* [24]. Flow curves of the sort shown in Figs. 2(a), 2(c), and 2(e) have been obtained by Pavlinek *et al.* [25] for electrorheological suspensions under electric fields and by Rodts *et al.* [12] for foams; the latter explained their shape by the fact that, due to the inhomogeneous nature of the shear field, an unsheared region occurs for shear stresses below a critical shear stress characterizing solid-liquid transition. The flow and corresponding deformation curves obtained in the present study all have a qualitatively similar shape, independent of the solid volume concentration, characterized by three different regions.

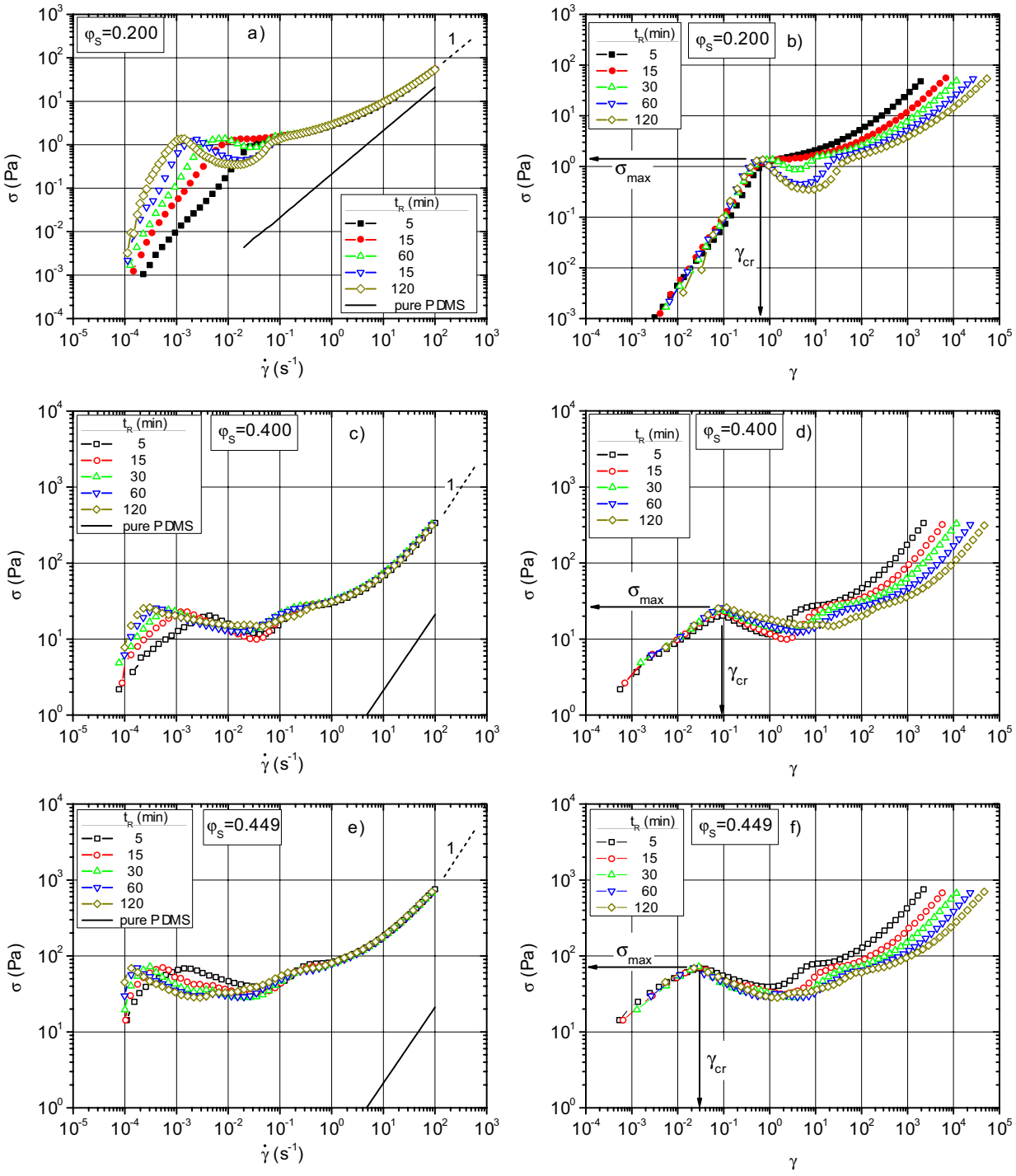

FIG. 2. (Color online) TCSR flow (a, c, e) and deformation curves (b, d, f) of the suspensions with solid volume concentrations of 0.200, 0.400, and 0.449 at various ramp times, t_R, inset. The corresponding flow curve for the pure carrier liquid is shown as a solid line.

(1) At low shear rates the flow curves increase monotonically up to a local maximum in shear stress, the increasing divergence between them revealing a distinct influence of the ramp time—namely, an increase in ramp time results in a shift to lower shear rates. The same data plotted as shear stress versus shear strain gives the corresponding deformation curves. These reveal monotonically increasing shear stresses, up to a local maximum value, σ_{max}, reached at a critical shear strain, γ_{cr}, are coincident and independent of the ramp time. The coincidence of the deformation curves, for each solid volume concentration, shows that the shear strain is the proper scaling in this region and the suspension behaves like a solid.

(2) At medium shear rates the flow curves decrease monotonically to reach a local minimum value in the shear stress before increasing again, showing once more a distinct influence of the ramp time. Also, in the deformation curves a region beyond the local maximum shear stress exists over

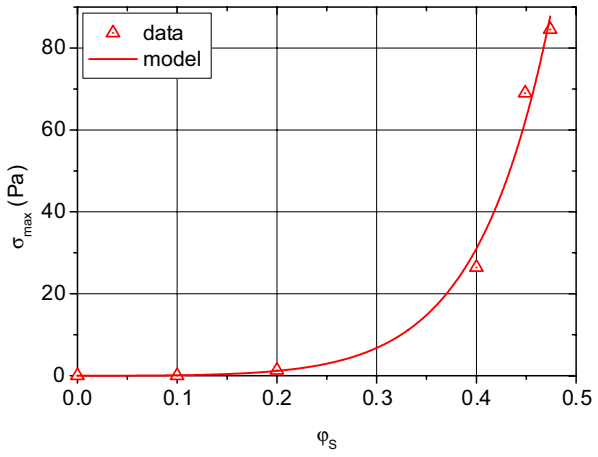

FIG. 3. (Color online) Maximum shear stress σ_{max} vs solid volume concentration φ_S for the long-term measurements. The flow and deformation curves for φ_S=0.100 and 0.474 have not been shown in Fig. 2.

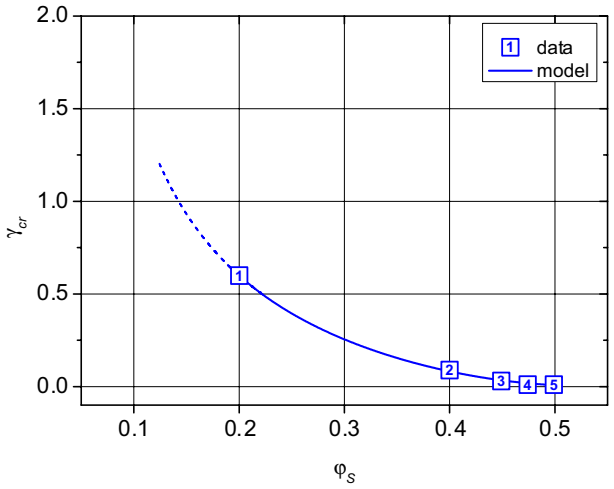

FIG. 4. (Color online) Critical shear strain γ_{cr} vs solid volume concentration φ_S. The deformation curves for solid volume concentrations of 0.474 (data point 4) and 0.499 (5) have not been shown in the paper.

which the shear stress continues to decrease through a local minimum before rising again; note the dependence on the ramp time. In this region neither the shear rate nor the shear strain are the correct strain measures. Hence the suspensions behave as hybrid materials.

(3) At high shear strains in the deformation curves the shear stresses increase monotonically, exhibiting an increasing divergence dependent on the ramp time. At high shear rates in the flow curves the monotonically increasing shear stresses are coincident for each solid volume concentration and independent of the ramp time—this provides clear evidence of liquidlike behavior at high shear rates, the highest value investigated showing that the flow curves become Newtonian-like, as indicated by the broken line with a slope of one [26]. Hence in this region the shear rate is the proper scaling and the suspension behaves like a liquid.

Before dealing with the transition region it is instructive to study the solidlike region in more detail. The coincidence of the deformation curves in the low shear strain region is clear evidence of a solidlike behavior due to direct interparticular contacts and particle network structures. At the lowest shear strains Hookean-like behavior can be observed due to the slope of the deformation curves which reaches a value of one. With increasing solid volume concentration the slope of the deformation curves in this region decreases, with a corresponding deviation from Hookean-like behavior. It is interesting to note that the deformation curves at low shear strains reach almost the same shear stress maximum, σ_{max}, at nearly the same critical shear strain, γ_{cr}, for a fixed solid volume concentration; the value of σ_{max} being greater the greater the solid volume concentration.

In Fig. 3, the dependence of the maximum shear stress on the solid volume concentration is shown for the long-term ramp time t_R=120 min [cf. Figs. 2(b), 2(d), and 2(f)]. The experimental data can be modeled by

$$\sigma_{max}(\varphi_S) = \sigma_0 \varphi_S^2 e^{(\varphi_S - \varphi_{cr})/\varphi_{cr}}, \quad (3)$$

where σ_0=12.019 Pa, φ_{cr}=0.1058, and the correlation coefficient r=0.9891. In Fig. 3 we clearly recognize that a critical solid volume concentration φ_{cr} is necessary for the appearance of maxima which is found to be 0.1058 in the model.

In Fig. 4 the dependence of the critical shear strain γ_{cr} [cf. Figs. 2(b), 2(d), and 2(f)] on the solid volume concentration φ_S is depicted. The experimental data have been modeled with an empirical exponential equation of the form

$$\gamma_{cr}(\varphi_S) = \frac{\varphi_{rcp}}{\varphi_S} e^{\varphi_{S,max}/(\varphi_S - \varphi_{S,max})}, \quad 0 < \varphi_S < \varphi_{S,max}, \quad (4)$$

where φ_{rcp}=0.6268, $\varphi_{S,max}$=0.5205, and the correlation coefficient r=0.9994. For $\varphi_S \to 0$ (pure carrier liquid) the expected behavior of an infinite critical shear strain is realized. The critical solid volume concentration $\varphi_{S,max}$ describes a maximum packing fraction of the disperse phase. For $\varphi_S \to \varphi_{S,max}$ the critical shear strain tends to zero, i.e., due to the intense interactions of the particles a deformation of the disperse phase is no longer possible. For the suspensions investigated here the value of φ_{rcp} was found to be close to the theoretically calculated maximum packing fraction of a random closed packing (index rcp) with monodisperse spherical particles ($2/\pi \approx 0.6366$). The value of $\varphi_{S,max}$ is in the vicinity of the packing fraction of a cubic arrangement of monodisperse spheres ($\pi/6 \approx 0.5236$, see, e.g., Cumberland and Crawford [27]).

The region between the solid state and the liquid state is of special interest because in this region neither pure solidlike nor pure liquidlike behavior is contained in the plots described above. In Fig. 5(a) the low-strain region of the curves corresponding to Fig. 2(b) are depicted in a linear plot as a function of the ramp time. The straight lines indicate the slope of the strain curves above the shear stress maximum. With growing ramp time the monotonous structural change tends to a nonmonotonous structural breakup displayed in an increasingly rapid stress drop.

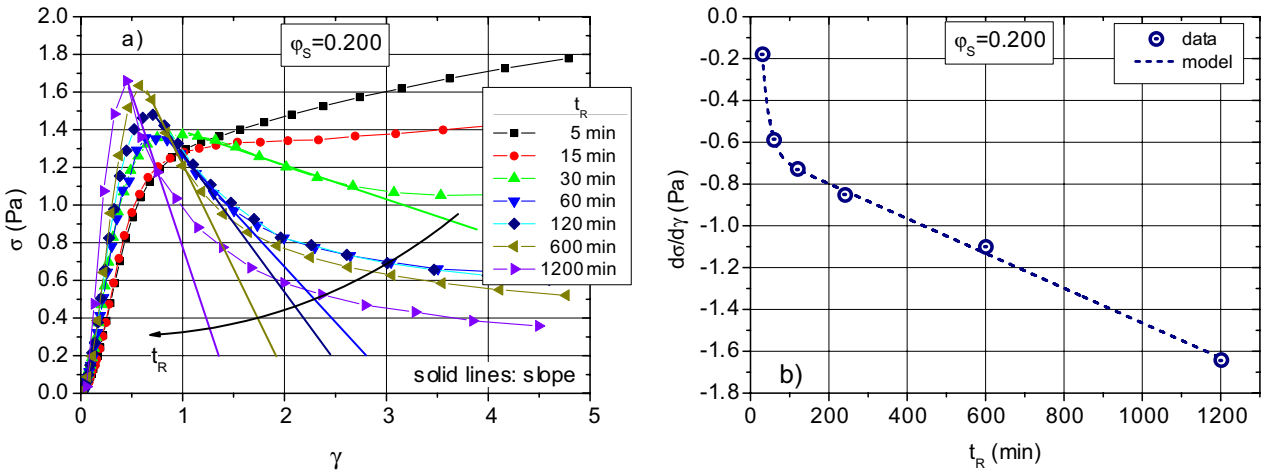

FIG. 5. (Color online) (a) Linear plot of the deformation curves in Fig. 2(b) and (b) fit curve of the slopes above the local shear stress maxima. To prevent overlap in (a) the curve with a ramp time of 240 min is not shown here.

The slopes of the experimental data, after reaching the local shear stress maximum in Fig. 5(a), are modeled in Fig. 5(b) by the empirical expression

$$\frac{\mathrm{d}\sigma}{\mathrm{d}\gamma} = \sigma_{m,\mathrm{cr}} e^{-t_R/t_{R,\mathrm{cr}}} + \dot{\sigma}_{m,\mathrm{cr}} t_R + A, \tag{5}$$

where $\sigma_{m,\mathrm{cr}}=2.368$ Pa, $t_{R,\mathrm{cr}}=18.741$ min, $\dot{\sigma}=-8.3\times10^{-4}$ Pa/min, $A=-0.6328$ Pa, and the correlation coefficient $r=0.9998$. Here, the parameter $t_{R,\mathrm{cr}}$ indicates the critical ramp time at which a local shear stress maximum in the deformation curves occurs for the first time. For the suspension shown in Fig. 5 this seems to be the case for a ramp time in the range between 15 and 30 min. The parameter $\dot{\sigma}_{m,\mathrm{cr}}$ characterizes the dependence of the rate of the instability for longer ramp times. Equilibrium pathways for other solid volume concentrations show the same behavior.

B. Transient controlled shear stress (TCSS) experiments

Figure 6 shows the flow curves and the corresponding deformation curves for suspensions measured in the TCSS mode for two solid volume concentrations at different ramp times. The ramp time t_R of the time-dependent shear stress ramp $\sigma(t)$ is defined according to Eq. (2) where the initial and final shear rates have been replaced by the initial and final shear stresses. The flow curves [Figs. 6(a) and 6(c)], are typical for liquids with a flow transition in the TCSS mode (see, e.g., [25]). At very low shear stresses, a "scattering" of the measured shear rate data occurs resulting from the solidlike behavior of the suspension. In this state no reasonable shear rate can be obtained by the rheometer. This is in accordance with the simulations by Varnik *et al.* [7] as well as with experiments of other authors (see, e.g., [24,25]).

A further increase of the shear stress up to a value below a critical plateau stress leads to a region in the flow curves where a clear dependence of the shear rate on the shear stress can be obtained.

In Fig. 6(c) we experience the effect of a shear softening ($d\sigma/d\dot{\gamma}>0$) followed by a shear hardening ($d\sigma/d\dot{\gamma}<0$), i.e., a change in the sign of $d\sigma/d\dot{\gamma}$. Similar effects have been found by Varnik *et al.* [7] (see Fig. 15 therein) by numerical simulations in the TCSS mode for a binary Lennard-Jones glass as well. The occurrence of a "nose" in the flow curve in Fig. 6(c) equates to an inflection point in the deformation curves [Fig. 6(d)].

The effect of the change in the sign of $d\sigma/d\dot{\gamma}$ corresponds to the observation of decreasing shear stresses with increasing shear rates in the TCSR mode [see Figs. 2(a), 2(c), and 2(e)]. However, in the TCSS mode this structural change takes place at higher solid volume concentrations. As shown in Fig. 6(a), at the lower solid volume concentration shear hardening is not observed. The corresponding deformation curves in Figs. 6(b) and 6(d) coincide increasingly below a distinct shear stress plateau which indicates a solidlike behavior of the suspensions in the low shear stress range.

Above the solidlike region transition takes place in a very narrow shear stress region where the shear rate increases nearly stepwise over more than two orders of magnitude. The stress drop (discontinuity) in the TCSR mode [see Fig. 5(a)] corresponds now in the TCSS mode to strain discontinuity. These observations confirm the theoretical results of Picard *et al.* [19] who found a destabilization process of the sample, caused by moving fronts of regions with low viscosity from the walls to the center of a (parallel plate) measuring geometry, as a reason for the intrinsic material instability.

For shear stresses above this plateau region the flow curves coincide independently of the ramp time and the deformation curves diverge. This indicates a liquidlike behavior of the suspensions which approach a Newtonian state with increasing shear stresses as shown in Figs. 6(a) and 6(c). Whereas a Newtonian behavior can be found for the lower solid volume concentration, it was not possible to reach this region for the higher solid volume concentration due to flow instabilities during the experiments.

C. Comparison of TCSR and TCSS experiments

The differences of the transition behavior in the TCSR and TCSS modes are given in Fig. 7 for two different ramp

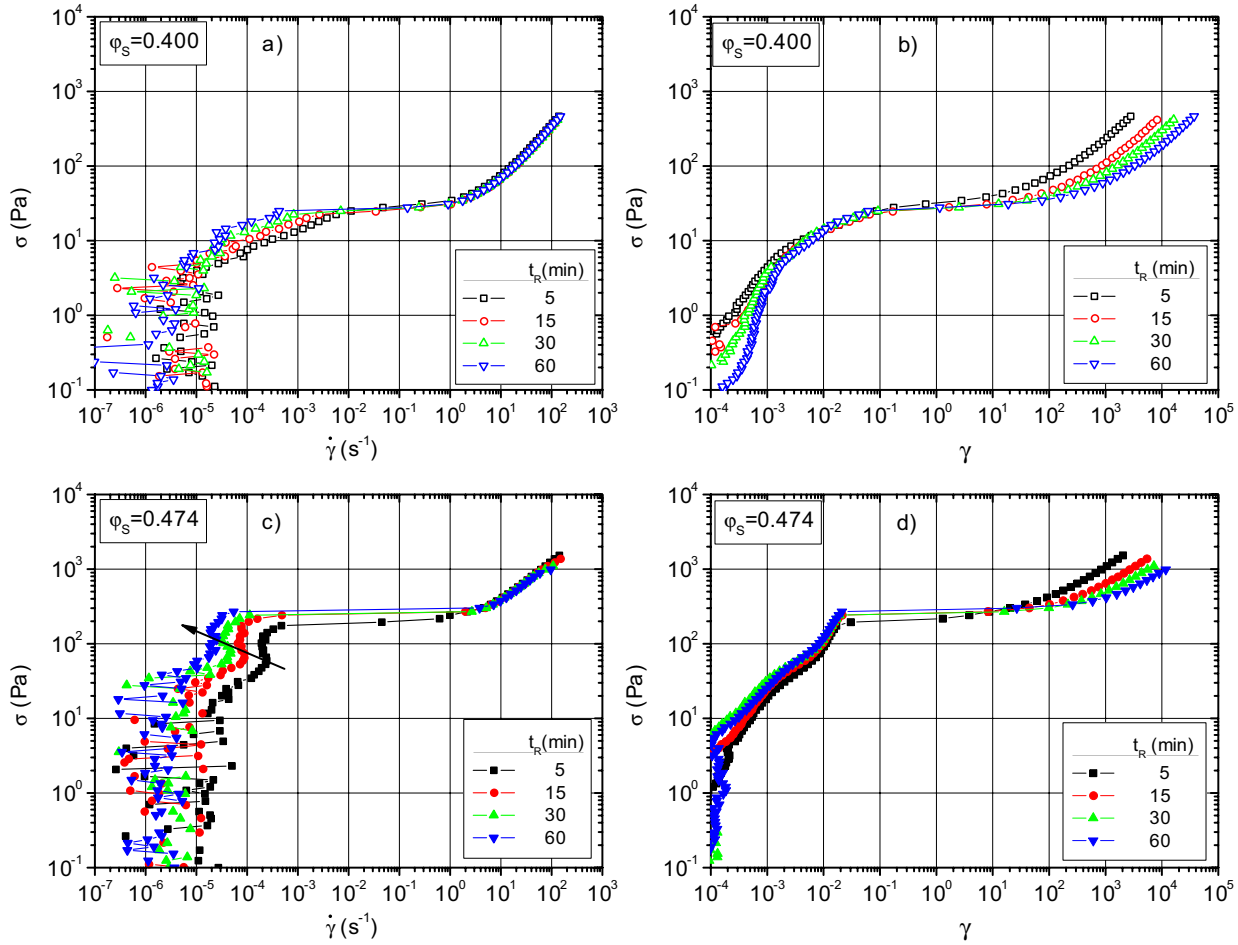

FIG. 6. (Color online) TCSS flow curves (a,c) and deformation curves (b,d) of suspensions with solid volume concentrations of 0.400 and 0.474 for different ramp times.

times and solid volume concentrations. One should be aware of the fact that in the TCSR mode the shear rate $\dot{\gamma}$ is given and the shear stress σ is the reaction of the material, hence $\sigma=f_{\mathrm{CSR}}(\dot{\gamma})$. In contrast to this, in the TCSS mode σ is given and $\dot{\gamma}$ is the reaction of the material, and hence $\dot{\gamma}=f_{\mathrm{CSS}}(\sigma)$. Later it is shown that f_{CSS} is not always the inverse of f_{CSR} and vice versa, e.g., $f_{\mathrm{CSS}} \neq f_{\mathrm{CSR}}^{-1}$. Nevertheless, for the sake of comparison the flow curves in both modes are given in the traditional form $\sigma=f(\dot{\gamma})$. The curves of the TCSS experiments generally lie above the TCSR ones. At low ramp times [Fig. 7(a)], the suspension with $\varphi_S=0.200$ shows an initial stress hardening. With increasing shear stresses the shear rate decreases initially, reaches a minimum, and increases further with the shear stress.

A similar effect occurs at the same solid volume concentration for the larger ramp time. This effect in the TCSS mode has also been reported by Da Cruz *et al.* [28] for foams and emulsions. At higher solid volume concentrations stress hardening cannot be achieved. For higher ramp times and higher solid volume concentrations [Fig. 7(b)] it is observed that the inner structure of the suspensions is more sensitive against a forced shear strain in the TCSR mode. Contrary to the shorter ramp times and lower solid volume concentrations, the decrease of the shear stress after the local maximum is more pronounced in the case of $\varphi_S=0.400$ (one should be aware of the fact that the flow curves in Fig. 7 are portrayed as a log-log plot). The subsequent increase to a local maximum shear stress and decrease to a local minimum shear stress in the flow curve occurring in the TCSR mode originates in an abrupt structural change due to the forced strain at a critical shear rate. In the TCSS mode this abrupt structural change corresponds to an almost jumplike increase of the shear rate if a critical shear stress is reached.

To understand the reaction of the suspension on the applied mode, the TCSR and TCSS curves are portrayed this time in a mathematically correct way in Fig. 8. The given quantity (independent variable) is plotted on the abscissa, the reaction of the material (dependent variable) is plotted on the ordinate. The symmetry line is $\sigma=K\dot{\gamma}$ with $K=1$ Pa s. In the liquidlike region the reaction of the suspensions in the TCSS and TCSR modes are the inverse of each other:

$$f_{l,\mathrm{CSS}} = f_{l,\mathrm{CSR}}^{-1}. \tag{6}$$

Hence we have here a perfect reflection symmetry. However, in the transition region the symmetry breaks and the reaction of the suspensions is noninvertible:

$$f_{\mathrm{tr,CSS}} \neq f_{\mathrm{tr,CSR}}^{-1}, \tag{7}$$

which increases with increasing solid volume concentration.

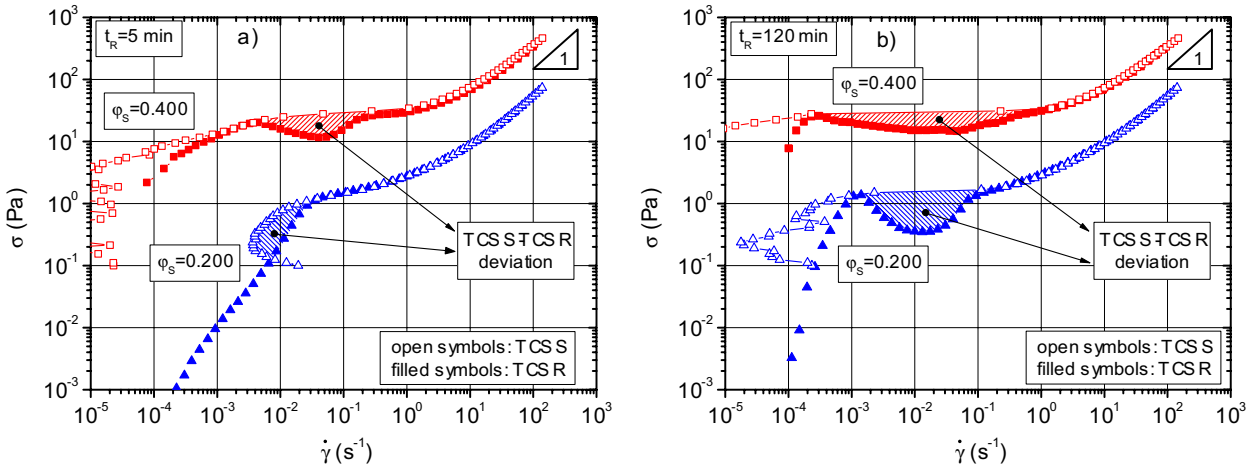

FIG. 7. (Color online) Comparison of the behavior of suspensions in TCSR and TCSS modes for solid volume concentrations of 0.200 and 0.400. The ramp times are (a) 5 min and (b) 120 min.

D. Solid-to-liquid versus liquid-to-solid transition

It has been stated that the suspensions show a solid-liquid transition, the experiments discussed in Secs. III A and III B having been performed with increasing shear rates and shear stresses, respectively. We address now the question of whether the solid-liquid transition is reversible, i.e., whether there is a difference between solid-liquid and liquid-solid transition. To determine this, experiments with a sequent increase and decrease of the shear rate or shear stress were carried out in order to gain deeper insights into structural changes during shear. Based on the very different behavior in TCSS and TCSR modes as shown in Sec. III C, the expectation was that the hysteretic behavior is also different in these modes. We focus on the long-term behavior and in Fig. 9 the up and down flow curves for the higher concentrated suspensions in the TCSR and TCSS modes are portrayed. The up curves in the TCSR mode [Fig. 9(a)], discussed above, are followed by monotonically decreasing down curves. At the lowest solid volume concentration (φ_S=0.100) the down curve does not reach a plateau value at the lowest shear rates investigated. The nonexistence of a plateau indicates a liquidlike behavior over the whole shear rate range. In contrast, the down curve for the next higher solid volume concentration (φ_S=0.200) shows a qualitatively different behavior. This curve approaches a nearly constant value at low shear rates and hence a permanent hardening during the shear occurs. Consequently, in the solid volume concentration range 0.100–0.200 the rheological behavior of the suspension changes significantly. The effects obtained for φ_S=0.200 are even more pronounced for the denser suspensions. These findings are in agreement with Fig. 3. In the TCSS mode the dense suspensions show a completely different behavior [Fig. 9(b)]. After an initial increase, the up curves lie, in all

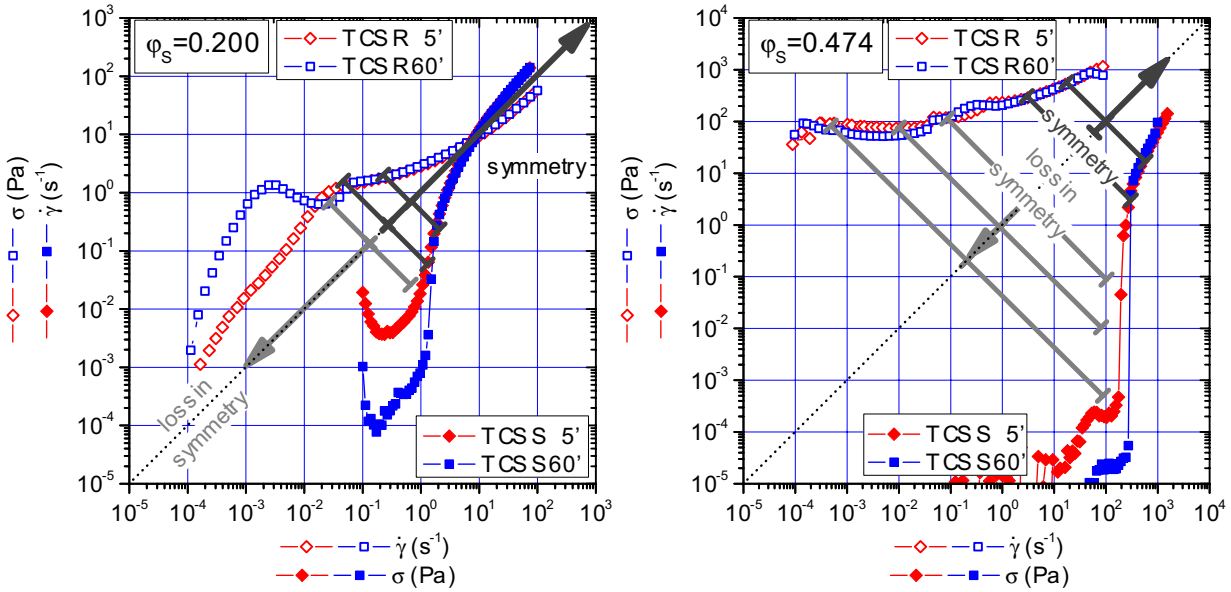

FIG. 8. (Color online) Symmetry chart of the TCSR and TCSS flow curves for suspensions with solid volume concentrations of (a) 0.200 and (b) 0.474 at different ramp times.

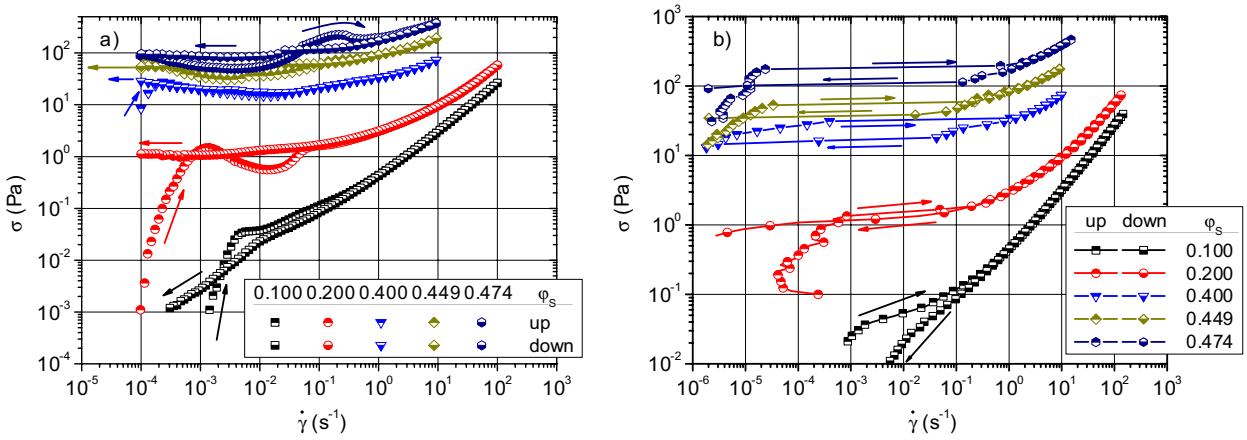

FIG. 9. (Color online) Hysteretic behavior of suspensions in TCSR (a) and TCSS (b) modes at various solid volume concentrations in the long-term behavior.

cases, above the down curves. Despite the fact that extremely low shear rates cannot be resolved by the rheometer, it is evident that the down curves reach plateau values at low shear rates. Furthermore, a distinct hysteresis is found for all solid volume concentrations. Again, these experimental observations agree qualitatively with the results of Picard *et al.* [19]. Moreover, the integration of the up and down curves shows that the hysteresis areas, i.e., the area between up and down curves, increase with increasing solid volume concentration. However, this effect is not immediately obvious due to the logarithmic plot of the data.

IV. CONCLUSIONS

A schematic of the reaction of suspension in the TCSR mode, for a fixed solid volume concentration, is portrayed in Fig. 10. In the start up region (I), from rest up to the critical shear strain γ_{cr}, a stable particle network structure forms in which the interparticular forces dominate over the hydrodynamic ones. Thus the particles arrange in "force chains" [18]. Such force chains have been observed experimentally by Radjai *et al.* [29] for photoelastic disks or, by numerical simulations, by Thornton [30] for polydisperse spheres. The interactions between the particles can be described globally

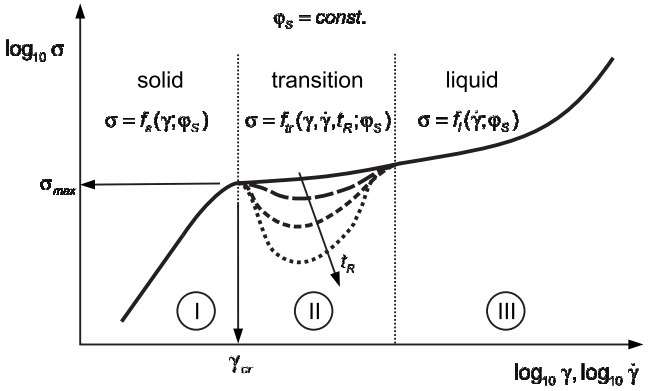

FIG. 10. Schematic of the deformation and flow behavior of dense suspensions at a fixed solid volume concentration.

by a Lennard-Jones potential [7]. For higher solid volume concentrations additional contact forces between the particles occur. In this regime the structure behaves like a solid, irrespective of the ramp time t_R, with the uniquely defined relation

$$\sigma = f_s(\gamma; \varphi_S = \text{const}). \tag{8}$$

At a fixed solid volume concentration the shear stress depends only on the shear strain, with the coincidence of the deformation curves at low shear strains being clear evidence of a solidlike (but not necessarily Hookean) behavior due to direct interparticular contacts and particle network structures. The reason why we can observe the start up is because the relaxation time λ of the suspension is much longer than the ramp time t_R, i.e., $\lambda \gg t_R$. Hence, the suspension is in "frozen equilibrium".

At the critical shear strain γ_{cr} the maximum strength σ_{max} of the particle network structure is reached, which is not stable to the applied shear strain. After passing through the maximum shear stress the network structure breaks down into clusters of particles or shear bands and the transition region II appears where solid and liquid states coexist. Inside the solid domains (force chains) the interactions between the particles are strong enough to resist to the flow-induced stress whereas the liquid domains undergo irreversible rearrangements of the remaining particle structures [7]. In this region the relation

$$\sigma = f_{\text{tr}}(\gamma, \dot{\gamma}, \ldots, t_R; \varphi_S = \text{const}) \tag{9}$$

holds, with the simultaneous dependence of the shear stress on the shear strain, shear rate, and ramp time complicating the modeling of this region.

With increasing shear strain or shear rate, the clusters break into particles until only single particles surrounded by liquid exist. Hence the suspension is completely fluidized. The coincidence of the flow curves in region III is clear evidence of this liquidlike behavior—hydrodynamic forces dominate over the interparticular forces and for a fixed solid volume concentration the suspension, irrespective of the ramp time t_R, behaves according to the unique relation

$$\sigma = f_l(\dot{\gamma}; \varphi_S = \text{const}). \quad (10)$$

The transition from solid to liquid state, e.g., the collapse of the particle network structure, is a dynamic process. In the limit of a very slow process compared to the relaxation time ($t_R \gg \lambda$), e.g., in the "equilibrium limit", the transition pathway is the energetically most favorable one because the deformation energy $\int \sigma d\gamma$ reaches a minimum. In a very quick process ($\lambda \gg t_R$) the solid structure collapses and goes over immediately to a liquid state with a vanishing transition regime.

The transition from a solid to liquid state is not equal to the transition from a liquid to solid state. Independent of TCSR or TCSS modes, the up and down curves do not coincide in the low shear region; showing that the static or particle network structure at rest and the dynamic particle network structures are quite different at the same low shear strain or low shear stress of the up and down curves.

The results of the TCSR and TCSS experiments show distinct differences in the low shear and transition region. In the TCSR mode, at low shear strains, the inner structure of the suspension is forced to deform and the resulting shear stress depends on the interparticular forces; in the TCSS mode the particle network is loaded with a given shear stress. Below a critical shear stress the network is simply deformed whereas above this range the suspension flows.

A basic necessary condition for the transition is the formation of a particle network structure, which is only possible if the particle concentration exceeds a critical value. The dependence of the transition on the (solid) particle volume concentration (cf. Fig. 3) can be interpreted as a "soft" bifurcation. Note that it was possible to cover the start up process due to the special composition of the suspensions we used.

ACKNOWLEDGMENTS

This research was supported by the Deutsche Forschungsgemeinschaft (Research Group FOR 608, Project 2). The PMMA particles were provided by Röhm GmbH & Co. KG (Darmstadt, Germany) which is gratefully acknowledged. The authors would like to thank Gabriele Jena and Markus Horn for their assistance in carrying out the extensive rheological measurements. We thank Professor P. H. Gaskell (Leeds, UK) and Professor M. Fuchs (Konstanz, Germany) for valuable discussions.

[1] S. Chander, Colloids Surf., A **133**, 143 (1998).
[2] H. A. Barnes and K. Walters, Rheol. Acta **24**, 323 (1985).
[3] J. P. Hartnett and R. Y. Z. Hu, J. Rheol. **33**, 671 (1989).
[4] G. Astarita, J. Rheol. **34**, 275 (1990).
[5] J. Schurz, J. Rheol. **36**, 1319 (1992).
[6] H. A. Barnes, in *Theoretical and Applied Rheology*, *Proceeding of the XI International Congress on Rheology, Brussels, Belgium, 1992*, edited by P. Moldenaers and R. Keunings Elsevier, Amsterdam, 1992), pp. 576–578.
[7] F. Varnik, L. Bocquet, and J.-L. Barrat, J. Chem. Phys. **120**, 2788 (2004).
[8] L. Zhu, N. Sun, K. Papadopoulos, and D. De Kee, J. Rheol. **45**, 1105 (2002).
[9] C. W. Macosko, *Rheology—Principles, Measurements, and Applications* (VCH, New York, 1994).
[10] D. Doraiswamy, A. N. Mujumdar, I.-L. Tsao, A. N. Beris, S. C. Danforth, and A. B. Metzner, J. Rheol. **34**, 647 (1991).
[11] P. C. F. Møller, J. Mewis, and D. Bonn, Soft Mater. **2**, 274 (2006).
[12] S. Rodts, J. C. Baudez, and P. Coussot, Europhys. Lett. **69**, 636 (2005).
[13] J. C. Baudez and P. Coussot, Phys. Rev. Lett. **93**, 128302 (2004).
[14] P. Coussot, J. S. Raynaud, F. Bertrand, P. Moucheront, J. P. Guilbaud, H. T. Huynh, S. Jarny, and D. Lesueur, Phys. Rev. Lett. **88**, 218301 (2002).
[15] F. Pignon, A. Magnin, and J.-P. Piau, J. Rheol. **40**, 573 (1996).
[16] H. B. Callen, *Thermodynamics and an Introduction to Thermostatistics*, 2nd ed. (Wiley, New York, 1985).
[17] J. D. Goddard, J. Non-Newtonian Fluid Mech. **102**, 251 (2002).
[18] J. D. Goddard, Annu. Rev. Fluid Mech. **35**, 113 (2003).
[19] G. Picard, A. Ajdari, L. Bocquet, and F. Lequeux, Phys. Rev. E **66**, 051501 (2002).
[20] V. A. Hackley and C. F. Ferraris, *The Use of Nomenclature in Dispersion Science and Technology* (National Institute of Standards and Technology, Washington, D.C., 2001), Special publication 960-3.
[21] L. Heymann, S. Peukert, and N. Aksel, J. Rheol. **39**, 697 (1995).
[22] M. D. Graham, J. Rheol. **39**, 697 (1995).
[23] K. Dullaert and J. Mewis, J. Colloid Interface Sci. **287**, 542 (2005).
[24] L. Heymann, S. Peukert, and N. Aksel, Rheol. Acta **41**, 307 (2002).
[25] V. Pavlinek, P. Sáha, J. Pérez-González, L. de Vargas, J. Steijskal, and O. Quadrat, Appl. Rheol. **16**, 14 (2006).
[26] J. J. Stickel and R. L. Powell, Annu. Rev. Fluid Mech. **37**, 129 (2005).
[27] D. J. Cumberland and R. J. Crawford, *The Packing of Particles* (Elsevier, Amsterdam, 1987).
[28] F. Da Cruz, F. Chevoir, D. Bonn, and P. Coussot, Phys. Rev. E **66**, 051305 (2002).
[29] F. Radjai, D. E. Wolf, M. Jean, and J. J. Moreau, Phys. Rev. Lett. **80**, 61 (1998).
[30] C. Thornton, Kona **15**, 81 (1997).